Economic Geology
Vol. 92, 1997, pp. 569–577

An Exsolution Origin for Low-Temperature Sulfides at the Hemlo Gold Deposit, Ontario, Canada

WAYNE G. POWELL[†] AND DAVID R. M. PATTISON

Department of Geology and Geophysics, University of Calgary, Calgary, Alberta, Canada T2N 1N4

Abstract

Many aspects of the timing and genesis of the Archean Hemlo gold deposit are unresolved; pre-, syn- and postmetamorphic models have been proposed. The presence of abundant low-temperature sulfide minerals within highly deformed, sillimanite-grade host rocks has been used to support a postmetamorphic origin for the deposit. However, the present Sb-As-Hg ore assemblage, including cinnabar-realgar-orpiment assemblages, developed through a sequence of exsolution events during postpeak metamorphic cooling. At peak metamorphism, most of the As and Hg, along with Tl, Cu, Zn, and minor Fe, was incorporated into a high-temperature antimonian sulfosalt. In the lower amphibolite facies or upper greenschist facies, impure (Hg, Zn)S exsolved from the high-temperature phase. An impure chalcopyrite and native antimony exsolved from the host sulfosalt soon after, leaving behind an Sb_2S_3-As_2S_3 solid solution. Further cooling resulted in the exsolution of cinnabar and mercurian sphalerite from the (Hg,Zn)S. Impurities in the cinnabar and chalcopyrite exsolved to form aktashite, arsenopyrite and native antimony. Eventually, orpiment exsolved from the arsenic-bearing stibnite. Late, retrograde events converted the free orpiment to realgar and remobilized the realgar over short distances, along with cinnabar and native antimony. The history of sequential sulfide exsolution, along with the deformed nature of the Sb-As-Hg-bearing veins, and their metamorphosed alteration selvages, suggests that the metals were introduced prior to, or during, peak metamorphism.

Introduction

WITH its estimated 20 million ounces (Moz) of gold, the Hemlo gold deposit of northwestern Ontario is the largest gold deposit currently being mined in Canada. In addition to its economic importance, Hemlo is of interest because of its atypical alteration style and metal associations, including Mo, As, Hg, and Sb. The highly deformed nature of the deposit and the high metamorphic grade of the host rocks has obscured many relationships at the mine site and has resulted in a broad spectrum of genetic models being proposed for the origin of the deposit. Currently discussed ideas for the genesis of Hemlo include premetamorphic porphyry mineralization (Kuhns et al., 1994; Johnston, 1996), syn- to postmetamorphic shear zone-related mineralization (Hugon, 1986; Corfu and Muir, 1989), and postmetamorphic multistage replacement mineralization (Pan and Fleet, 1995).

The relative timing of metamorphism and ore deposition is an important but unresolved aspect of the deposit's history. There is an apparent mismatch of low- to moderate-temperature sulfide minerals, such as realgar, orpiment, cinnabar, and stibnite, with host rocks of sillimanite grade. The estimated peak-metamorphic temperature of 600°C exceeds the melting temperatures of these minerals: 307°C for realgar (Clark, 1960), 315°C for orpiment (Kirkinskiy et al., 1967), <345°C for cinnabar (Dickson and Tunell, 1959), and 556°C for stibnite (Pettit, 1964).

This paper addresses the origin of Sb-As-Hg-mineralization in the Hemlo deposit and its relationship to regional metamorphism. The distribution and textures of sulfide assemblages, along with associated alteration, provide constraints on the timing of gold mineralization at the Hemlo deposit.

[†] Corresponding author: email, wpowell@telusplanet.net

General Geology

The Hemlo gold deposit is located in the Hemlo-Schreiber greenstone belt of the Superior province, northwestern Ontario. Since production began in 1985, the three mines that exploit the deposit (Williams mine, Golden Giant mine, and David Bell mine) have produced 9.5 million ounces (Moz) of gold and account for one-quarter of Canada's gold production.

The main ore zone lies on the edge of a quartz-feldspar porphyritic rock, interpreted to be intrusive in origin (Moose Lake porphyry; Kuhns et al., 1994; Johnston, 1996), within a highly deformed sequence of metasedimentary and metavolcanic strata. Felsic volcanic rocks have been dated at 2772 ± 2 Ma (Corfu and Muir, 1989a). In the mine area, the strata are oriented at an average of 115° to 65° N. Granodioritic plutons intruded the supracrustal rocks between 2688 and 2678 Ma (Corfu and Muir, 1989).

Metamorphosed alteration associated with the deposit includes a central zone of microcline, commonly barian, surrounded by a zone of muscovite. A more extensive zone of aluminum enrichment is defined by an increased abundance of aluminosilicates with respect to the regional, unaltered metasedimentary rocks (Kuhns et al., 1986; Johnston, 1996).

Gold is spatially associated with microcline alteration, and Au grades correlate strongly with Mo. In general, the deposit is also enriched in Sb, As, Hg, Tl, Ba, V, and B. However, metals are broadly zoned across the deposit. Arsenic, mercury, and thallium are all confined to the central part of the deposit. These metals are nearly absent from the northwest downplunge extension of the Williams mine, where there is

0361-0128/97/1935/569-9$6.00

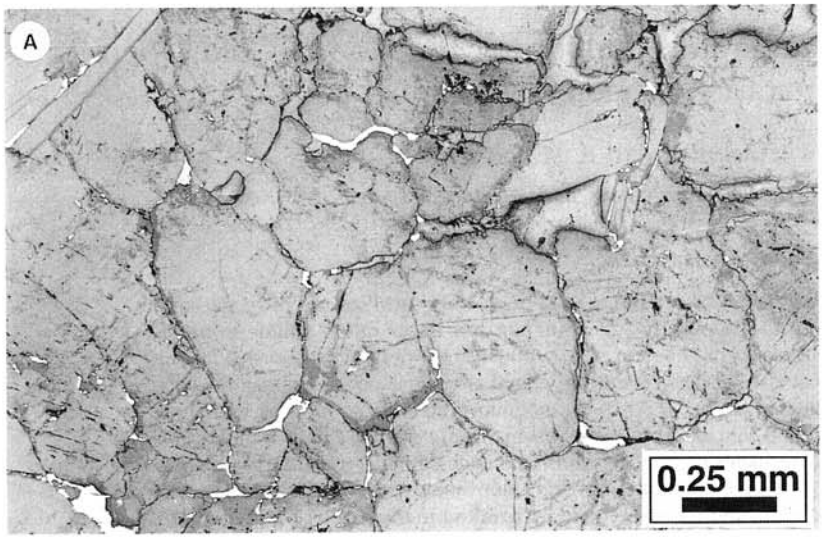
A
0.25 mm

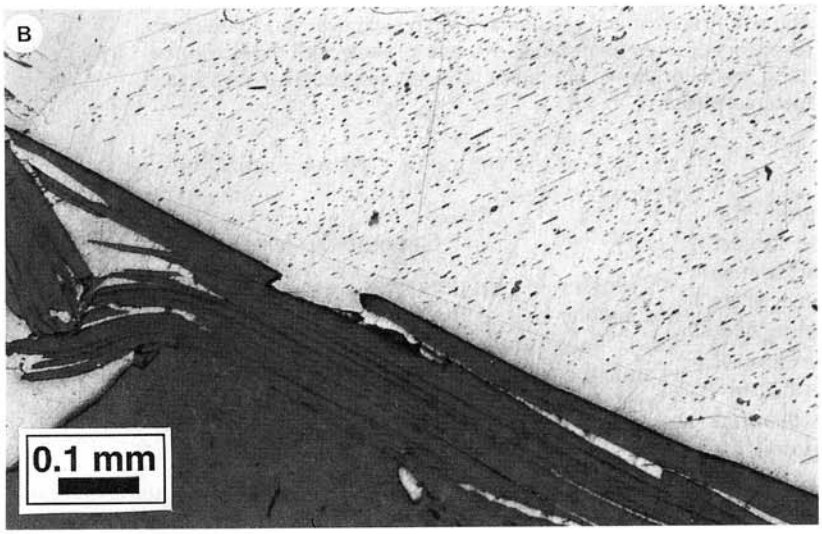
B
0.1 mm

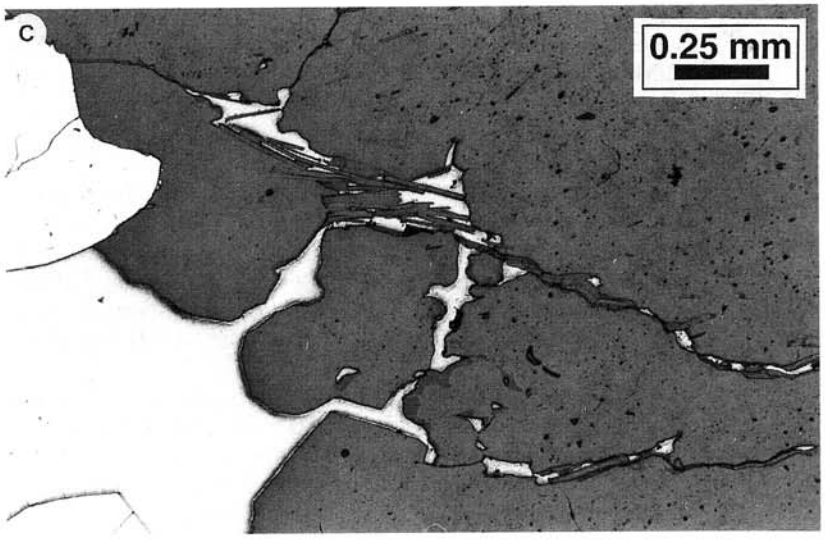
C
0.25 mm


D
0.1 mm

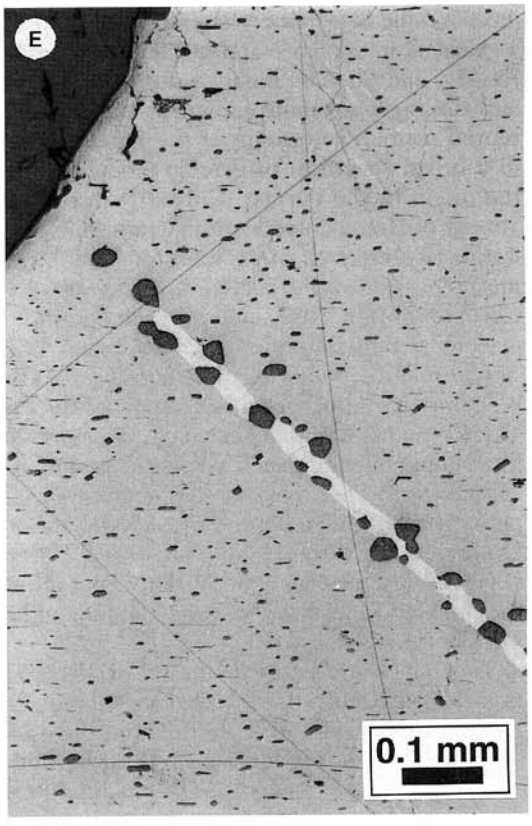
E
0.1 mm

an increased abundance of the base metal minerals galena, chalcopyrite, and sphalerite (Harris, 1989).

Harris (1989) documented a diverse assemblage of Sb-As-Hg-bearing minerals at Hemlo. Most are rare, very fine grained (<5 μm), and often occur in complex intergrowths. Tables of electron microprobe analyses of many of these minerals can be found in the appendix of Harris (1989). Stibnite, realgar, and cinnabar are the most abundant minerals containing these metals.

The Hemlo-Schreiber greenstone belt is multiply deformed. Several researchers have discussed the regional tectonic history of the area (e.g., Kuhns et al., 1994; Muir, 1997), and Michibayashi (1995) documented the detailed structural evolution of the Golden Giant mine. The tectonic history proposed by Kuhns et al. (1994) is favored and summarized below. The earliest recognized structural elements are isoclinal folds associated with a bedding-parallel foliation. These folds are premetamorphic. The predominant structural element in the Hemlo area is a set of large-scale, east-west-trending, shallowly plunging isoclinal folds with a strong axial planar cleavage. These synmetamorphic folds are parallel to the margin of the Pukaskwa batholith that marks the southern boundary of the greenstone belt. Small dextral folds affect the predominant axial-planar foliation. This dextral-shear event developed late in the metamorphic history. Northwest-striking brittle faults with dextral displacement are associated with overprinting greenschist facies retrograde mineral assemblages (Kuhns et al., 1994).

The metamorphic history of the Hemlo area is not yet well documented. However, local studies have been undertaken at the David Bell mine site and on a showing 5 km to the east. Burk et al. (1986) and Pan and Fleet (1993) reported peak metamorphic conditions of approximately 600°C and 4.5 kbars based on analyses of sillimanite-bearing rocks. Both groups of workers reported higher pressure estimates from kyanite-bearing assemblages (>6 kbars) and agreed that sillimanite postdates kyanite, but disagreed on the temperature of formation of the sillimanite. Burk et al. (1986) interpreted the kyanite to have developed during peak metamorphism, followed by sillimanite growth on the retrograde path during isothermal uplift. Pan and Fleet (1993) suggested that the belt is polymetamorphic, with a high-temperature sillimanite-grade event superimposed on an earlier lower temperature kyanite-grade assemblage. Repeated retrograde hydrothermal events affected the belt, producing localized greenschist and subgreenschist facies calc-silicate assemblages (Pan and Fleet, 1992; Kuhns et al., 1994). These assemblages include unusual mineral compositions such as antimonian vesuvianite (Pan and Fleet, 1992).

U/Pb dating of titanite from unmineralized rock suggests that peak metamorphism occurred ca. 2677 Ma (Corfu and Muir, 1989). Protracted cooling of the deposit is suggested by $^{40}Ar/^{39}Ar$ dating of hornblende (closure ca. 2645 Ma), muscovite (closure ca. 2615 Ma), and biotite (closure ca. 2570 Ma) from upper levels of the mines (Grant, 1986). Retrograde hydrothermal events are suggested by U/Pb ages of 2643 to 2632 Ma from monazite and rutile (Corfu and Muir, 1989).

Description and Interpretation of Selected Ore Assemblages

Common Sb-As-Hg ore assemblages

Stibnite and native antimony are the most common Sb-bearing minerals in the Hemlo deposit. Stibnite has been recognized as being emplaced late in the structural history of the deposit (Michibayashi, 1995). Fine-grained, anhedral stibnite grains are disseminated within bands throughout micaceous and feldspathic ore. They occur most commonly in triple junctions between granoblastic quartz feldspar grains (Fig. 1A), along grain boundaries, and along cleavage planes in mica crystals (Fig. 1B). Coarse-grained stibnite occurs in various structural traps, including tension fractures, pressure shadows, and fold noses (Fig. 1C).

The most common occurrence of native antimony is in the form of globular (often radiating) grains <50 μm in diameter. Most are aligned along fractures and as patches of disseminated native antimony that are associated with realgar and stibnite. Native antimony also commonly occurs as discontinuous crusts on large stibnite grains and decreases in abundance with distance from these grains.

Realgar and orpiment are the most abundant As-bearing minerals and occur in several distinct forms. Very fine grained realgar (<10 μm) is disseminated along wispy fractures in boudinaged quartz veins (Fig. 1D). Realgar also occurs as fine-grained inclusions within granoblastic microcline. Realgar-coated fractures are common adjacent to these realgar-rich veins and pods. Orpiment is less common. It is found in habits similar to realgar, as well as occurring as aligned inclusions in large stibnite grains (Fig. 1E). Arsenopyrite occurs as euhedral crystals that are commonly included in stibnite and/or disseminated in realgar-stibnite-bearing gangue matrix.

Cinnabar is the most common Hg-bearing mineral. Cinnabar is always associated with realgar and stibnite and is very commonly associated with chalcopyrite and sphalerite, cinnabar being complexly intergrown with the latter. Very fine grained (<10 μm) cinnabar is disseminated throughout realgar-rich veins and patches. The textures and occurrence of cinnabar is very similar to realgar, including its presence as aligned inclusions in large stibnite grains. Mercury is also found in a number of sulfosalts including tetrahedrite-tennantite and aktashite, as well as in solid solution in gold and sphalerite.

FIG. 1. Common textures of abundant Sb- and As-bearing minerals. A. Stibnite, with minor native Sb, along grain boundaries and in triple junctions in a granoblastic feldspar matrix (reflected light). B. Stibnite along cleavage planes in muscovite. Large stibnite grain (top) contains orpiment inclusions (reflected light). C. Stibnite extending from a large grain along fractures and feldspar grain boundaries (reflected light). D. Vein quartz with wispy fractures coated with very fine grained realgar and cinnabar (plane-polarized light). E. Twinned stibnite grain with orpiment inclusions aligned along cleavage planes and twin planes (reflected light).

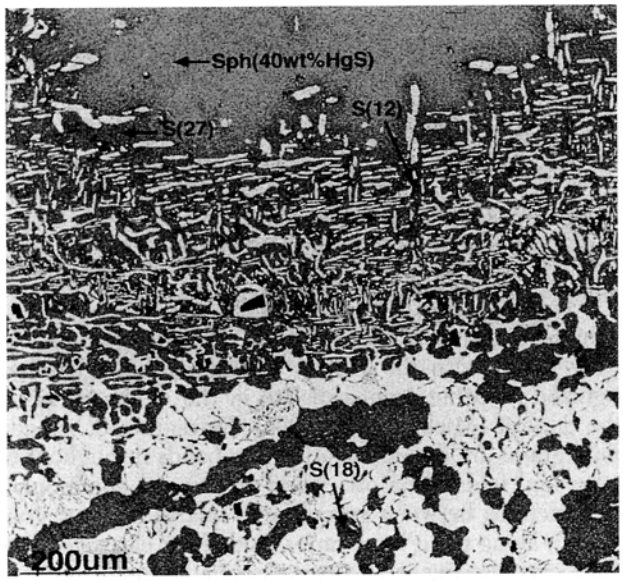

FIG. 2. Hg X-ray map of sphalerite(sph)-cinnabar intergrowth in sample G1. Cinnabar is white, pyrite is black, and sphalerite is in darkening shades of gray corresponding to decreasing Hg content. Arrows point to analysis points in sphalerite with wt % HgS in parenthesis, e.g., S(18).

Metal ratios vary greatly throughout the deposit. Although there are many similarities in sulfide assemblages, there are also striking differences due to the variance in metal ratios throughout the deposit. Therefore, it is necessary to discuss the specific mineralogical-textural relationships in a set of key samples with different metallic compositions: Hg-Zn rich (sample W1), Hg-Tl rich (sample GG25), and Hg-Cu rich (samples W2 and W3). Detailed descriptions of the textures and mineralogical relationships are essential to understand the genesis of these minerals.

Hg–Zn-rich ore assemblages (sample W1)

Sample W1 is a muscovite schist from the Williams mine A zone that contains a 10-cm-wide, boudinaged quartz vein oriented parallel to the schistosity. Fine-grained pyrite is common in bands parallel to the foliation. Coarse-grained stibnite is concentrated between quartz boudins. Minor stibnite, native antimony, and cinnabar are disseminated through the schist and also occur in late fractures adjacent to the quartz vein.

Pyrite, stibnite, and native antimony are disseminated throughout the vein quartz, where they occur along fractures, grain boundaries, and subgrain boundaries. Grains of realgar and minor cinnabar, generally less than 10 μm in diameter, occur along closely spaced, regularly oriented, annealed fractures. This fine-grained, but abundant realgar imparts a characteristic orange to pink-brown color to these veins.

Massive, coarse-grained stibnite occurs in the space between quartz boudins. Aligned, elliptical orpiment inclusions (5–30 μm) comprise approximately 5 percent of each large stibnite grain. These inclusions are most abundant along twin planes and cleavage planes (Fig. 1E). In order of decreasing abundance, stibnite grains also contain rare inclusions of cinnabar, native arsenic, and chalcopyrite. Native arsenic and cinnabar are commonly intergrown within inclusions.

The crystallographic control of inclusion distribution suggests that these inclusions exsolved from a predominantly Sb_2S_3-As_2S_3 solid solution. Exsolved orpiment then coalesced along weaknesses within the stibnite crystal structure.

Cinnabar-sphalerite intergrowths occur on the edge of a large patch of massive stibnite between two quartz boudins. The largest cinnabar-sphalerite grain (1 cm diam) is zoned, both texturally and compositionally (Fig. 2). The core is 3 mm in diameter and is composed of iron-free mercurian sphalerite (up to 40 wt % HgS). Annealed fractures in the grain core are marked by bands of Hg depletion and irregular trails of both euhedral pyrite and cinnabar grains that contains sphalerite inclusions.

The sphalerite core is surrounded by a 0.3- to 0.8-mm-wide, sphalerite-rich zone. This zone is composed of fine, elongate inclusions of cinnabar (30%) arranged in a gridlike pattern controlled by the crystallographic structure of the sphalerite matrix. This sphalerite is moderately mercurian (26 wt % HgS). The larger cinnabar inclusions (up to 20 μm in width) each contain round to wormlike inclusions of sphalerite.

The external zone of the composite grain is 3 to 6 mm wide and is composed of a coarser grained intergrowth of cinnabar (77%) and sphalerite (23%) that contains 24 wt percent HgS. The cinnabar grains again contain abundant wormy inclusions of sphalerite. The sphalerite inclusions contain 18 wt percent HgS.

The sphalerite-cinnabar intergrowth textures described above, along with the decreasing Hg content of sphalerite from core to rim, are consistent with a history of exsolution of sphalerite and cinnabar from an initial HgS-ZnS solid solution, as would be predicted from experimentally derived phase diagrams for the HgS-ZnS system (Dini et al., 1995). At conditions corresponding to the amphibolite facies and upper greenschist facies, HgS and ZnS formed a complete solid solution. During cooling of a grain of composition

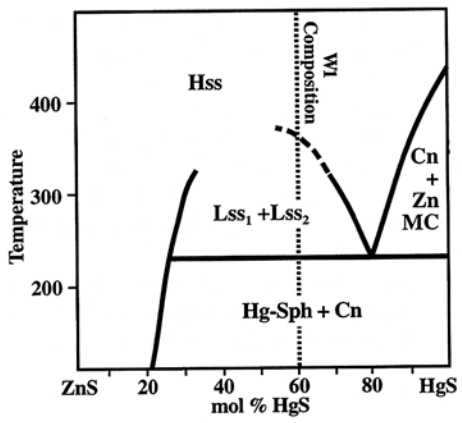

FIG. 3. Experimentally based ZnS-HgS phase diagram (P = 3.5 kbars). The dotted line corresponds to the integrated composition of the cinnabar-sphalerite grain in W1. Hss = high-temperature solid solution, Lss = low-temperature solid solution, ZnMCn = zincian metacinnabar. Modified from Dini et al. (1995).

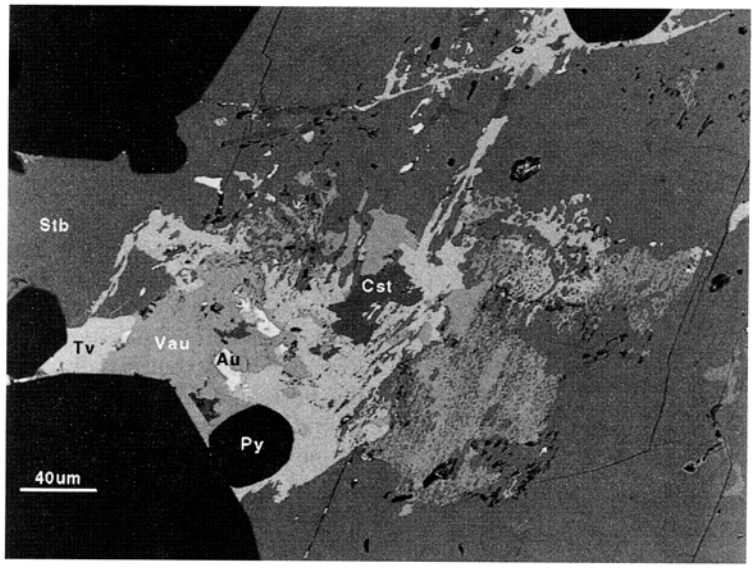

FIG. 4. Backscattered electron image of mineral intergrowths within large stibnite (Stb) grain in sample G1. Note the spongelike intergrowth of vaughanite (Vau) and tvalchrelidzeite (Tv) with stibnite. Other minerals include pyrite (Py), chalcostibite (Cst), and native gold (Au).

$Hg_{0.6}Zn_{0.4}S$ (integrated composition of the grain described above), at moderate pressure, the high-temperature solid solution would have reached a solvus in the mid-greenschist facies (Fig. 3). The solid solution then exsolved into two low-temperature solid solutions, one that is ZnS rich and the other HgS rich. Upon further cooling into the subgreenschist facies, a peritectic was reached at which time the Hg-rich solid solution exsolved to form low Hg sphalerite inclusions within pure cinnabar.

Hg-Tl-rich ore assemblages (sample GG25)

GG25 is a sample originally collected and described by Harris (1989; drill hole GG25, 336.1 m). One-half of the sample is a sugary feldspathic rock with disseminated pyrite; it contains seams rich in pyrite and vanadian muscovite. Small stibnite grains occur throughout the feldspathic rock, but one large stibnite grain is of particular interest. This 3-mm grain lies within a small quartz pod within the feldspathic host rock.

It exhibits very subtle, patchy compositional zoning, with irregular patches of low As stibnite contained within a grain that is predominantly As free. In addition to aligned orpiment inclusions (1%), the grain includes larger, patchy inclusions of several rare minerals. In order of abundance these are vaughanite ($TlHgSb_4S_7$) (Harris et al., 1989), tvalchrelidzeite ($Hg_{12}(Sb, As)_8S_{15}$), chalcostibite ($CuSbS_2$), and native gold. Vaughanite and tvalchrelidzeite tend to form intergrown masses that are commonly elongate parallel to stibnite twin planes. Outlying inclusions commonly have a spongelike texture, with stibnite filling the interstices (Fig. 4). Elongate inclusions trail off from the larger masses along stibnite twin planes. Chalcostibite occurs at the periphery of vaughanite-tvalchrelidzeite masses as stubby or elongate inclusions also lying along stibnite twin planes.

The sponge texture of both vaughanite and tvalchrelidzeite within the stibnite is strong evidence for exsolution of these minerals from the stibnite host. The spatial association of chalcostibite and gold with these exsolution intergrowths also supports an exsolution origin for these minerals. The interdigitation of all of the exsolved minerals suggests that they exsolved at approximately the same time. Prior to exsolution, this grain must have been an antimonian sulfosalt that contained significant quantities of Hg, Tl, As, Cu, and Au (in decreasing order).

Hg-Cu-rich ore assemblages (samples W2 and W3)

Both W2 and W3 come from the Williams mine A zone. These samples contain boudinaged and fractured quartz veins that occur within a muscovite schist matrix; they have similar sulfide textures and associations. Coarse-grained stibnite grains occur within extension veins and pinched veins (i.e., late tectonic veins and early, deformed veins). These grains contain aligned, elliptical orpiment inclusions and rare inclusions of chalcopyrite and cinnabar. Cinnabar is present in some boudin necks. Realgar and cinnabar occur as grains <10 μm in diameter that occur along wispy, annealed fractures throughout the vein quartz.

Intergrowths of chalcopyrite and cinnabar dot the rims of large stibnite grains, along with native antimony. Contacts are irregular and interfingering. Cinnabar grains commonly contain wormy inclusions of mercurian sphalerite, similar to those described in W1, or are rimmed by mercurian sphalerite with irregular contacts (Fig. 5A). Aktashite ($Cu_6Hg_3(As,Sb)_4S_{12}$) occurs as interdigitated rims along chalcopyrite crystal boundaries (Fig. 5A). Aktashite inclusions also commonly occur in cinnabar (Fig. 5B). W2 contains pure chalcopyrite. However, within W3 pure chalcopyrite is intergrown with antimony-bearing chalcopyrite (0.7 wt % Sb) in a diffuse and wispy fashion (Fig. 5C), and aktashite inclusions are spatially associated with the antimony-bearing chalcopyrite.

As in samples W1 and GG25, the abundant orpiment inclu-

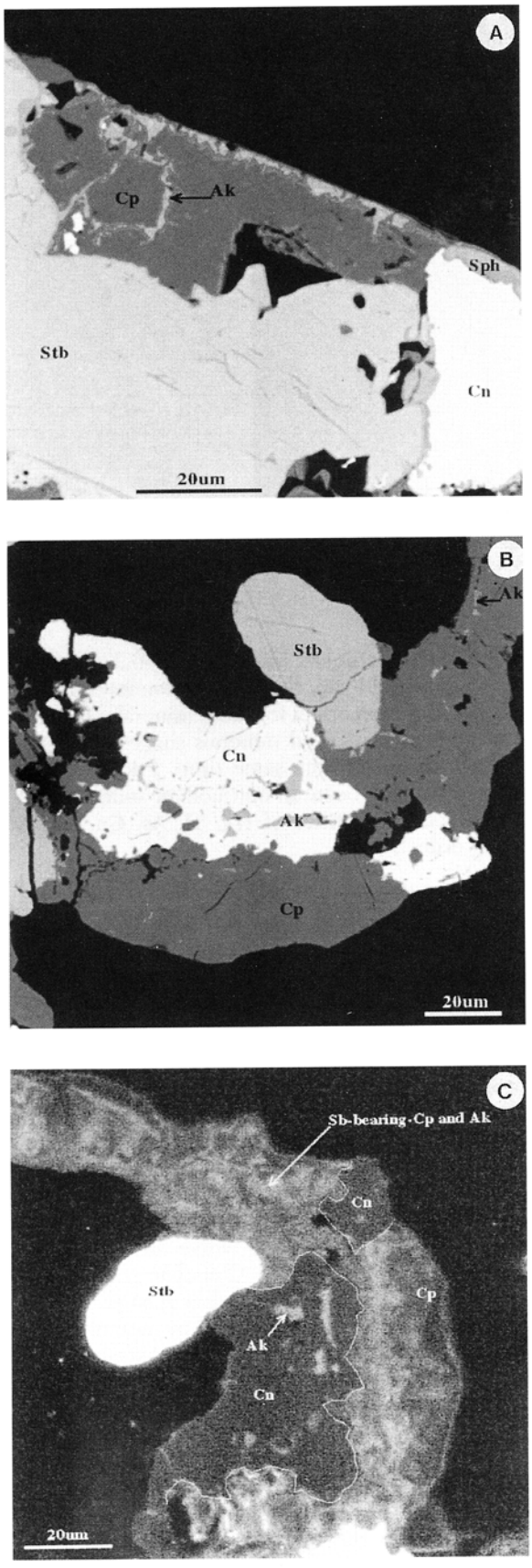

sions within coarse-grained stibnite have clearly exsolved from the stibnite. The similarity in occurrence of orpiment, cinnabar, and chalcopyrite inclusions within stibnite supports the interpretation that the chalcopyrite and cinnabar intergrowths which occur on the edge of the stibnite grains also originated as exsolution blebs. The fact that most of the Cu and Hg sulfides occur at the margins, whereas orpiment is still abundant within the stibnite, suggests that the Cu and Hg sulfides exsolved earlier than orpiment.

Intergrowths of chalcopyrite and cinnabar have not been observed within inclusions in stibnite, whereas the association of these two minerals is very common on stibnite rims. Therefore, it is likely that two distinct sulfide phases exsolved from the host, one Cu rich and the other Hg rich. Both phases migrated to the vein margins and accumulated together in embayments, fractures, and other structural traps. Both the copper and mercury sulfides later expelled impurities. The exsolution of aktashite and sphalerite left grains of chalcopyrite and cinnabar. Chalcopyrite grains with abundant aktashite inclusions, and grains with wispy Sb impurity associated with aktashite inclusions, probably represent samples frozen at different stages of exsolution and internal diffusion.

Gold in relation to Sb-As-Hg minerals

Gold is commonly associated with mercury-, antimony-, and arsenic-bearing phases and geochemical studies have shown a strong correlation of Au with As, Sb, and Hg (Thode et al., 1991). The most common form of gold at Hemlo is a gold-mercury alloy, with reported mercury contents as high as 27 wt percent (Harris, 1989). Another example of gold-mercury association was observed in sample GG25, where native gold (no detectable Hg) is interleaved with cinnabar. Each wispy cinnabar and gold layer is less than 1 μm thick (Fig. 6A). Clearly the intergrowth formed as a result of exsolution from an Au-Hg sulfide.

Gold is commonly associated with Sb in the form of aurostibite ($AuSb_2$, Harris, 1989). In GG25, native gold grains occur throughout the complex intergrowth of antimonian minerals (stibnite, vaughanite, and tvalchrelidzeite). The gold grains have complex forms and interfinger with the host minerals (Fig. 6B). If the gold had simply been present as inclusions in the sulfide host during metamorphism, then more regular forms with lower surface area to volume ratios would be expected. Instead, the shape and distribution of these native gold grains is consistent with their exsolution along with Hg- and Tl-bearing minerals from a high-temperature solid solution sulfide phase.

Arsenic has not been reported in solid solution with gold, but native arsenic commonly rims native gold grains (Fig.

FIG. 5. Mineral intergrowths in the Hg-Cu-rich samples, W2 and W3. A. Backscattered electron image of mineral intergrowths on the edge of a large stibnite (Stb) grain in W2. Cinnabar (Cn) is rimmed and interdigitated with sphalerite (Sph). Chalcopyrite (Cp) is interdigitated with aktashite (Ak) along grain boundaries. B. Backscattered electron image of mineral intergrowths in an embayment along a stibnite extension fracture in W3. Chalcopyrite and cinnabar both contain inclusions of aktashite. C. Sb X-ray map corresponding to image in B. Note the wispy intergrowth of Sb-free and Sb-bearing chalcopyrite.

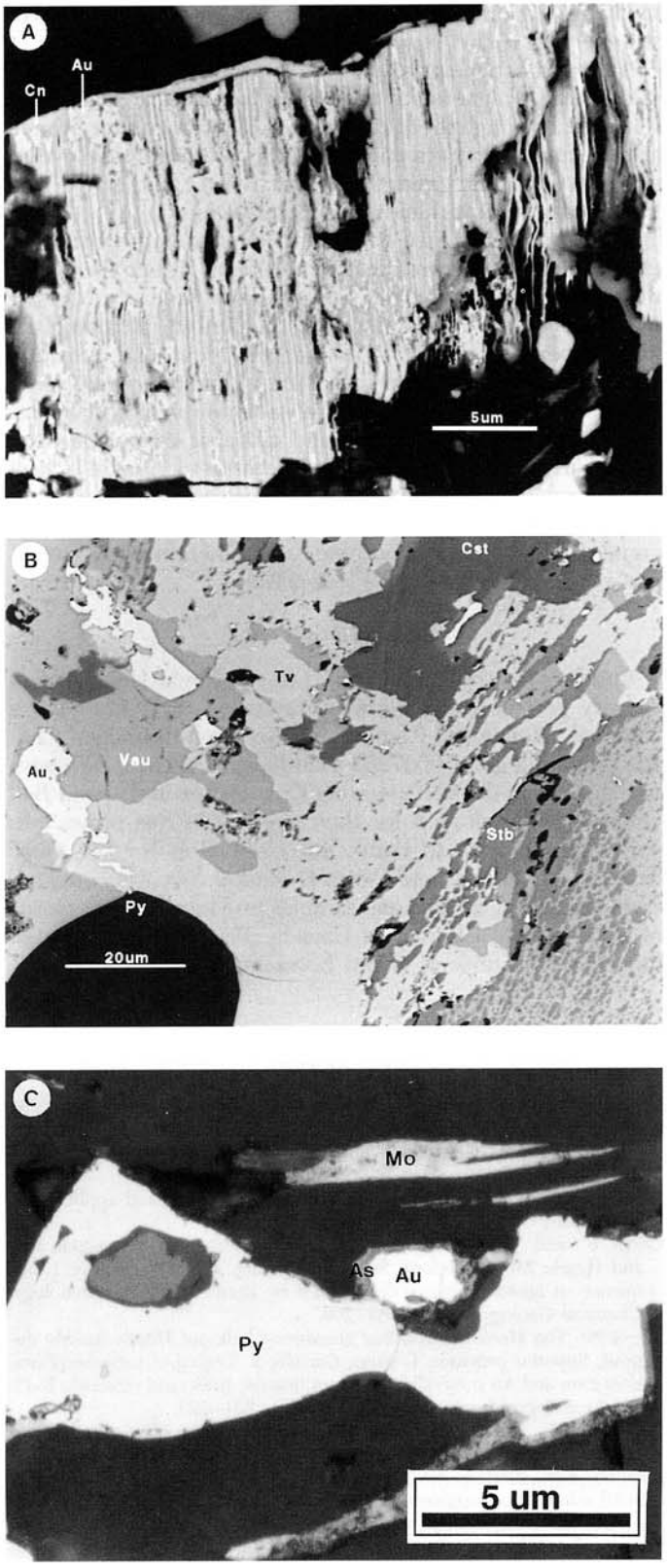

FIG. 6. Intergrowth textures of native gold with Hg-, Sb-, and As-bearing minerals. A. Fine laminated intergrowth of gold (Au) and cinnabar (Cn) in G1. B. Irregular gold grains associated with exsolution intergrowths in G1. See Figure 4 for mineral abbreviations. C. Native gold (Au) rimmed by native arsenic (As). Note that there is no native arsenic rim on neighboring pyrite (Py) or molybdenite (Mo) grains.

6C). In these samples arsenic does not rim neighboring pyrite or molybdenite grains. The most likely explanation for these relationships is that the native arsenic exsolved from a high-temperature gold-arsenic alloy. Due to the microscopic scale of the gold grains, the arsenic migrated completely from the gold core.

Origin of Present Sb-As-Hg Assemblages

Sb-As-Hg mineralization is associated with highly deformed quartz veins and pods that cut the disseminated gold ore (Kuhns et al., 1994). The veins are extensively boudinaged in the plane of the synmetamorphic foliation. Some of these deformed, mineralized quartz veins have an associated aluminous alteration envelope that is metamorphosed to an assemblage of coarse-grained kyanite + quartz + muscovite with overprinting sillimanite (Powell and Pattison, 1997). Accordingly, the Sb-As-Hg veins must postdate the Au-Mo ore, but predate, or be synchronous with, peak metamorphism and its accompanying deformation. And yet, these relatively volatile metals are still present and experienced only very limited metamorphic and postmetamorphic remobilization.

Principles that govern the metamorphism of silicate rocks are also applicable to the sulfide assemblages. Melting of a single mineral rarely occurs in natural metamorphic rocks because reactions with other minerals occur at lower grades during prograde metamorphism. If the sulfides were present prior to, or during, metamorphism, then it is expected that there will have been metamorphic reactions that consumed the low-temperature sulfide minerals and produced minerals stable at elevated pressure and temperature.

There are no relict assemblages of premetamorphic Sb-As-Hg assemblages at Hemlo, so one can only speculate as to the exact sulfide assemblages which were present prior to regional metamorphism. However, because of the complex composition of the ores, the slow cooling history of the belt, and the fact that retrogression of sulfide assemblages does not require reintroduction of water to the rock, a fairly detailed history of retrograde processes is recorded in Hemlo's sulfide assemblages.

At peak metamorphic conditions, the sulfide mineral assemblage was far simpler than the present assemblage. Most of the As and Hg were incorporated into an antimonian sulfosalt, along with Cu, Zn, and minor Fe, Tl, and Au. The composition of individual grains of the high-temperature sulfosalt would have been dependent upon local metal ratios, and so would have varied across the deposit. Unfortunately, it is not possible to reconstruct the composition of any particular high-temperature sulfosalt grains based on the composition and abundance of exsolution phases because of the small-scale migration of many of these minerals.

Deducing more exactly the identity of the most likely high-temperature mineral, based on comparison with available experimental studies of sulfide phase equilibria, is also impossible due to the limited applicability of these experiments to

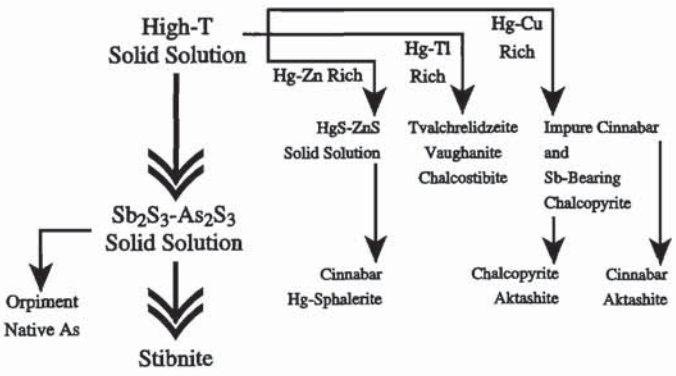

FIG. 7. Schematic illustration of post-peak metamorphic exsolution sequence in Sb-As-Hg sulfides at the Hemlo deposit.

conditions at Hemlo. Whereas experimental studies approach the peak metamorphic temperature of 600°C reached at Hemlo, most experiments are undertaken at lower pressures than those that prevailed at Hemlo (approx 7 kbars; Burk et al., 1986). Furthermore, with seven or more components, the compositions of the high- to moderate-temperature natural solid solution phases at Hemlo were far more complex than those that have been studied in the laboratory.

The high-temperature As-Hg-Cu-Zn-Fe antimonian sulfosalt was most likely very ductile at peak metamorphic conditions. It flowed readily over short distances during deformation and accumulated in local low-pressure zones, such as pressure shadows between boudins or extension fractures.

During cooling the high-temperature sulfosalt sequentially exsolved a number of sulfide phases. This sequence is illustrated schematically in Figure 7. The earliest phase to exsolve was probably an Hg-Zn sulfide that included small amounts of Cu, Fe, As, and Sb. A Cu-Fe sulfide that included small amounts of Hg, Sb, and As (i.e., an impure chalcopyrite) must have exsolved from the host grain shortly after. Exsolution of native antimony accompanied the solution of the sulfide phases. Variations in local composition resulted in variations in the mineral species exsolved from the host grain. For example, high-temperature Hg-bearing sulfosalts that were Tl rich and Zn poor exsolved vaughanite and tvalchrelidzeite. All three phases migrated through the host grains, either amassing within the host grain or on its margin.

Continued cooling into the greenschist facies resulted in secondary exsolution. The Hg-Zn sulfide separated into cinnabar and mercurian sphalerite. Aktashite, arsenopyrite, and native antimony grew when trace Cu, Fe, As, and Sb were no longer stable in solution in the Hg-Zn sulfide phase. Similarly, aktashite exsolved from the impure chalcopyrite when the Hg, As, and Sb could no longer be contained in the chalcopyrite structure.

After the expulsion of sulfides of Hg, Cu, Zn, Fe, and Tl, the remaining mineral was a solid solution of stibnite and orpiment. Solid solution of Sb_2S_3 and As_2S_3 has been noted from experimental studies conducted at 200° to 300°C (Moore and Dickson, 1973; Dickson et al., 1974) and in Carlin-type deposits, but are otherwise rare in nature. In most cases at Hemlo, orpiment was later exsolved from this intermediate-temperature host mineral, leaving pure stibnite, or stibnite with a low As content.

Although orpiment is common as inclusions in large stibnite grains, realgar is the most abundant arsenic sulfide disseminated through the Hemlo ores. Realgar may have formed at the expense of orpiment during the late retrograde events that mobilized fine-grained cinnabar, realgar, and native antimony along fractures and grain boundaries.

The scenario outlined here does not claim to describe and explain all of the diverse ore assemblages at Hemlo. However, the retrograde-metamorphic exsolution origin of many of the most abundant exotic minerals in the deposit, including the low-temperature phases of realgar, orpiment, and cinnabar, does explain the apparent mismatch of low-temperature ore minerals with high-temperature metamorphic host rocks. Thus the presence of realgar and cinnabar cannot be cited to support postmetamorphic mineralization at Hemlo. In fact, the extended history of sequential exsolution that finally resulted in the development of realgar, orpiment, and cinnabar argues against postmetamorphic replacement models such as that proposed by Pan and Fleet (1995).

Acknowledgments

Funding for this project was provided by a University of Calgary post-doctoral fellowship awarded to W.G.P. and a National Science and Engineering Research Council of Canada operating grant 0037233 awarded to D.R.M.P. We wish to thank the Williams Operating Corporation and David Bell Operating Corporation for their support of this project. In particular we wish to thank Jim Gray, Rob Reukel, Gord Skrecky, Al Guthrie, and Pierre Desaultel. We also benefited from discussion, advice, and samples provided by Don Harris of the Geological Survey of Canada. This manuscript benefited from the reviews of two *Economic Geology* referees.

February 19, July 9, 1997

REFERENCES

Burk, R., Hodgson, C.J., and Quartermain, R.A., 1986, The geological setting of the Teck-Corona Au-Mo-Ba deposit, Hemlo, Ontario, Canada, *in* MacDonald, A.J., ed., Gold '86: Willowdale, Ontario, Konsult International, p. 311–326.

Clark, L.A., 1960, The Fe-As-S system: Phase relations and applications: ECONOMIC GEOLOGY, v. 55, p. 1345–1381.

Corfu, F., and Muir, T.L., 1989, The Hemlo-Heron Bay greenstone belt and Hemlo Au-Mo deposit, Superior province, Ontario, Canada: 1. Sequence of igneous activity determined by zircon U-Pb geochronology: Chemical Geology, v. 79, p.183–200.

——1989, The Hemlo-Heron Bay greenstone belt and Hemlo Au-Mo deposit, Superior province, Ontario, Canada: 2. Timing of metamorphism, alteration and Au mineralization from titanite, rutile and monazite U-Pb geochronology: Chemical Geology, v. 79, p. 201–223.

Dickson, F.W., and Tunell, G., 1959, The stability relations of cinnabar and metacinnabar: American Mineralogist, v. 44, p. 471–487.

Dickson, F.W., Radtke, A.S., Weissberg, B.G., and Heropoulos, C., 1974, Solid solutions of antimony, arsenic and gold in stibnite (Sb_2S_3), orpiment (As_2S_3) and realgar (As_2S_2): ECONOMIC GEOLOGY, v. 69, p. 383–390.

Dini, A., Benvenuti, M., Lattanzi, P., and Tanelli, G., 1995, Mineral Assemblages in the Hg-Zn-(Fe)-S system at Levigliani, Tuscany, Italy: European Journal of Mineralogy, v. 7, p.417–427.

Grant, J.W., 1996, $^{40}Ar/^{39}Ar$ geochronology of the postmetamorphic thermal history of the Hemlo area: Unpublished M.Sc. thesis, Queen's University, Kingston, Ontario, 281 p.

Harris, D.C., 1989, The mineralogy and geochemistry of the Hemlo gold deposit, Ontario: Canada Geological Survey Economic Geology Report 38, p. 88.

Harris, D.C., Roberts, A.C., and Criddle, A.J., 1989, Vaughanite ($TlHgSb_4S_7$), a new mineral from the Hemlo deposit Hemlo, Ontario, Canada: Mineralogical Magazine, v. 52, p. 691–697.

Johnston, P., 1996, Geological setting of the Hemlo gold deposit, Ontario, Canada: Unpublished Ph.D. thesis, Queen's University, Kingston, Ontario, 297 p.

Kirkinskiy, V.A., Ryaposov, A.P., and Yakushev, V.G., 1967, Phase diagram for arsenic tri-sulfide up to 20 kilobars: Isvestiia Akademiia Nauk USSR, v. 3, p. 1931–1933.

Kuhns, R.J., Sawkins, F.J., and Ito, E., 1994, Magmatism, metamorphism and deformation at Hemlo, Ontario, and the timing of Au-Mo mineralization in the Golden Giant mine: ECONOMIC GEOLOGY, v. 89, p. 720–756.

Michibayashi, K., 1995, Two phase syntectonic gold mineralization and barite remobilization within the main ore body of the Golden Giant mine, Hemlo, Ontario, Canada: Ore Geology Reviews, v. 10, p. 31–50.

Moore, D.E., and Dickson, F.W., 1973, Phases of the system Sb_2S_3-As_2S_3: American Geophysical Union Fall Meeting, p. 1223–1224.

Muir, T.L., 1997, Precambrian geology, Hemlo gold deposit area: Ontario Geological Survey Report 289, 219 p.

Pan, Y., and Fleet, M.E., 1995, The Late Archean Hemlo gold deposit, Ontario, Canada: A review and synthesis: Ore Geology Reviews, v. 9, p. 455–488.

——1992, Calc-silicate alteration in the Hemlo deposit, Ontario: Mineral assemblages, P-T-X constraints, and significance: ECONOMIC GEOLOGY, v. 87, p. 1104–1120.

Pan, Y., Fleet, M.E., and Stone, W.E., 1991, Skarn mineralization (Cr, Fe, Au) in an Archean greenstone belt, White River property, Hemlo area, Ontario: ECONOMIC GEOLOGY, v. 86, p. 1626–1645.

Pettit, F.S., 1964, Thermodynamic and electrical investigations on molten antimony sulfide: Journal of Chemical Physics, v. 38, p. 9–20.

Powell, W.G., and Pattison, D.R.M., 1997, Pre-metamorphic mineralization at the Hemlo gold deposit: Evidence from sulfide and silicate assemblages [abs.]: Geological Association of Canada Abstract Volume 22, p. 121.

Thode, H.G., Ding, T., and Crocket, J.H., 1991, Sulphur-isotope and elemental geochemistry studies of the Hemlo gold mineralization, Ontario: Sources of sulphur and implications for the mineralization process: Canadian Journal of Earth Sciences, v. 28, p. 13–25.